Scandinavian Journal of Statistics Theory and Applications

Scandinavian Journal of Statistics
doi: 10.1111/sjos.12026

Discrete Multicolour Random Mosaics with an Application to Network Extraction

M.N.M. VAN LIESHOUT

CWI, Amsterdam, The Netherlands

ABSTRACT. We introduce a class of random fields that can be understood as discrete versions of multicolour polygonal fields built on regular linear tessellations. We focus first on a subclass of consistent polygonal fields, for which we show Markovianity and solvability by means of a dynamic representation. This representation is used to design new sampling techniques for Gibbsian modifications of such fields, a class which covers lattice-based random fields. A flux-based modification is applied to the extraction of the field tracks network from a Synthetic Aperture Radar image of a rural area.

Key words: consistent polygonal field, dynamic representation, linear network extraction, Markov properties, random field

In memory of Tomasz F. Schreiber.

1. Introduction

In the 1980s, Arak and Surgailis introduced a class of planar Markov fields whose realizations form a coloured tessellation of the plane. The basic idea is to use the lines of an isotropic Poisson line process as a skeleton on which to draw polygonal contours with the restriction that each line cannot be used more than once. Note that many tessellations can be drawn on the same skeleton, and that the contours may be nested. The polygons are then coloured randomly subject to the constraint that adjacent ones must have different colours. Formally, the probability distribution of such polygonal Markov fields is defined in terms of a Hamiltonian with respect to the law of the underlying Poisson line process, which can be chosen in such a way that many of the basic properties of the Poisson line process (including consistency, Poisson line transects and an explicit expression for its probability distribution on the hitting set of bounded domains) carry over and a spatial Markov property holds. Another useful feature is that a dynamic representation in terms of a particle system is available. See Arak & Surgailis (1989, 1991) for further details and Arak *et al.* (1993) or Thåle (2011) for alternative point rather than line-based models. The special case where all vertices have degree three is studied by Mackisack & Miles (2002).

The simplest and most widely studied example of a planar Markov field is the Arak process (Arak 1982) which consists of self-avoiding closed polygonal contours. Hence, interaction is restricted to a hard core condition on the contours, and there are exactly two colourings using the labels 'black' and 'white' such that adjacent polygons have different colours. For the Arak process, the Hamiltonian is proportional to the total contour length by a factor two. One may introduce further length interaction by changing the proportionality constant. Doing so, Nicholls (2001) and Schreiber (2006) consider the separation between the black and white regions as the interaction gets stronger; Van Lieshout & Schreider (2007) develop perfect simulation algorithms for these models. For the more general case in which both length

and area terms feature in the Hamiltonian, Schreiber (2005) proposes a Metropolis–Hastings scheme based on the dynamic representation of the Arak process, which Kluszczyński *et al.* (2005) adapts and implements to solve foreground/background image segmentation problems. An anisotropic Arak process can be defined through local activity functions instead of the length functional (Schreiber, 2008, 2010) and allows for increased flexibility while preserving desirable basic properties including a dynamic representation. This representation forms the basis of a stochastic optimization algorithm in the context of image segmentation, implemented by Matuszak & Schreiber (2012), and helps to gain insight into the higher-order correlation structure.

Polygonal Markov field models with contours that may also be joined by a vertex of degree three or four (Arak & Surgailis, 1989, 1991) are much less well-understood because of the more complicated interaction structure. Papers in this direction include those by Clifford & Middleton (1989), by Clifford & Nicholls (1994), by Kluszczyński *et al.* (2007) and by Paskin & Thrun (2005).

In a previous paper (Schreiber & Van Lieshout 2010), we introduced a class of binary random fields that can be understood as discrete counterparts of the two-coloured Arak process. The aim of the present paper is to extend this construction to allow for an arbitrary number of colours and to relax the assumption of Schreiber & Van Lieshout (2010) that no polygons of the same colour can be joined by corners only. Our construction is two-staged: first, a collection of lines is fixed to serve as a skeleton for drawing polygonal contours (a regular lattice being the generic example), then the resulting polygons are coloured in such a way that adjacent ones do not have the same colour. The analogy with continuum polygonal Markov fields is exploited to define Hamiltonians that are such that the desirable properties of these processes mentioned previously hold. Moreover, we propose new simulation techniques that combine global changes with the usual local update methods employed for random fields on finite graphs (Winkler 2003). It should be stressed, though, that the discrete models considered in this paper are not versions of continuum polygonal Markov fields conditioned on having their edges fall along a given collection of lines.

The plan of this paper is as follows. In Section 2, we define a family of admissible multicolour polygonal configurations built on regular linear tessellations and define discrete polygonal fields with special attention to consistent ones. In Section 3, we present a dynamic representation of such consistent polygonal fields, which is used to prove the main properties of such models. In Section 4, we exploit the dynamic representation to develop a simulation method. The method is generalized to arbitrary Gibbs fields with polygonal realizations and applied to the detection of linear networks in images in Section 5. We conclude with a discussion.

2. Random fields with polygonal realizations

First, recall the definition of a regular linear tessellation by Schreiber & Van Lieshout (2010).

Definition 1. A *regular linear tessellation* of the plane is a countable family $\mathcal{T}$ of straight lines in $\mathbb{R}^2$ such that no three lines of $\mathcal{T}$ intersect at one point, and such that any bounded subset of the plane is hit by at most a finite number of lines from $\mathcal{T}$.

For a bounded open convex set D, $\mathcal{T}$ induces a partition of D into a finite collection $D_{\mathcal{T}}$ of convex cells of polygonal shapes, possibly chopped off by the boundary ∂D. In the succeeding text, we shall always assume that the boundary ∂D of D contains no intersection points of lines from $\mathcal{T}$, and that the intersection of each line $l \in \mathcal{T}$ with ∂D consists of exactly two points. To each line l, we ascribe a fixed activity parameter $\pi_l \in (0, 1)$ to allow for the possibility to favour some lines over others.

The next step is to assign a colour to each of the convex cells in the partition of D induced by the lines in $\mathcal{T}$. Write $\{1, \ldots, k\}$ for the set of colour labels. In this paper, we concentrate on the case that $k > 2$. Such a colouring gives rise to a planar graph whose edges are formed by the boundaries between cells that have been assigned different colours and whose vertices are the points at which the edges intersect each other or the boundary of D. For technical convenience, we shall assume that edges are open, that is, they do not contain the vertices. Faces of the graph, which are unions of cells of $D_{\mathcal{T}}$, are said to be adjacent if they share a common edge.

Definition 2. The family $\hat{\Gamma}_D(\mathcal{T})$ of *admissible coloured polygonal configurations* in D built on $\mathcal{T}$ consists of all coloured planar graphs $\hat{\gamma}$ in the topological closure $\overline{D} = D \cup \partial D$ of D such that

- all edges lie on the lines of $\mathcal{T}$;
- all interior vertices, that is, those lying in D, are of degree 2, 3 or 4;
- all boundary vertices, that is, those lying on ∂D, are of degree 1;
- no adjacent faces share the same colour.

Throughout this paper, the notation γ is used for (admissible) planar graphs, and the hat notation $\hat{\gamma}$ for the graph with colours assigned to its faces. In this notation, $\Gamma_D(\mathcal{T})$ stands for the family of all planar graphs γ arising as interfaces between differently coloured faces in $\hat{\gamma} \in \hat{\Gamma}_D(\mathcal{T})$. Note that for the case $k = 2$ treated by Schreiber & Van Lieshout (2010), all interior vertices have degree two. Vertices of degree two are also known as V-vertices, those of degree three as T-vertices and vertices of degree four as X-vertices.

To avoid confusion, it is important to distinguish between $D_{\mathcal{T}}$ and the members of $\Gamma_D(\mathcal{T})$, even though they all partition D. In the sequel, we shall reserve the terms 'segments' and 'nodes' for the former and 'edges' and 'vertices' for the latter. Thus, nodes are intersection points of lines in $\mathcal{T}$, which are joined by segments. Edges of γ are maximal unions of connected collinear segments that are not broken by other such segments lying on the graph (corresponding to vertices of degree three or four). Primary edges are maximal unions of connected collinear segments, possibly consisting of multiple edges due to T- or X-vertices. Likewise, a vertex of γ is a point where two edges of γ meet or where an edge of γ meets the boundary ∂D, nodes lying on the interior of graph edges are not considered to be vertices. These concepts are illustrated in Figure 1. The family $\mathcal{T}$ consists of two orthogonal line bundles and induces diamond-shaped cells. One element of $\Gamma_D(\mathcal{T})$ is plotted in Figure 1. Consider the polygonal face indicated by 'C' that is chopped off by the boundary. There are two boundary vertices and

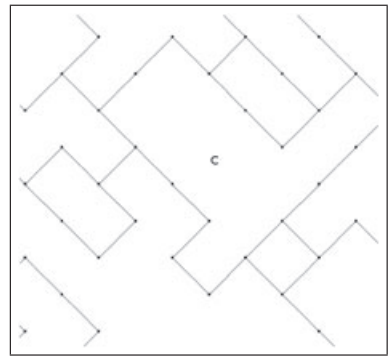

Fig. 1. Admissible polygonal configuration discussed in the text.

12 interior vertices, five of degree two, seven of degree three and none of degree four. We count 17 nodes on 16 complete segments, with two segments partly visible because of truncation by the boundary; C has 13 edges and its boundary lies on 8 primary edges. Note that in the literature, primary edges are sometimes also known as sides. See for example Weiß & Cowan (2011) for a discussion on nomenclature for tessellations and Calka (2010) or Van Lieshout (2012) for recent reviews of models.

We are now ready to define (discrete) polygonal fields.

Definition 3. Let $\mathcal{T}$ be a regular linear tessellation and ascribe fixed activity parameters $\pi_l \in (0,1)$ to the lines $l \in \mathcal{T}$. For a function $\mathcal{H}_D : \hat{\Gamma}_D(\mathcal{T}) \mapsto \mathbb{R} \cup \{+\infty\}$, the *(discrete) polygonal field* $\hat{\mathcal{A}}_{\mathcal{H}_D}$ with Hamiltonian $\mathcal{H}_D$ is the random element in $\hat{\Gamma}_D(\mathcal{T})$ for which

$$\mathbb{P}\left(\hat{\mathcal{A}}_{\mathcal{H}_D} = \hat{\gamma}\right) = \frac{\exp(-\mathcal{H}_D(\hat{\gamma}))\prod_{e\in E^*(\gamma)}\pi_{l[e]}}{\mathcal{Z}[\mathcal{H}_D]}. \tag{1}$$

Here $E^*(\gamma)$ denotes the set of primary edges in γ, and $l[e] \in \mathcal{T}$ is the straight line containing the open edge e.

The constant

$$\mathcal{Z}[\mathcal{H}_D] = \sum_{\hat{\theta}\in\hat{\Gamma}_D(\mathcal{T})} \exp(-\mathcal{H}_D(\hat{\theta})) \prod_{e\in E^*(\theta)} \pi_{l[e]} \tag{2}$$

that ensures that $\mathbb{P}$ is a probability distribution and is called the partition function. Note that the polygonal field is a Gibbs field with Hamiltonian

$$\mathcal{H}_D(\hat{\gamma}) - \sum_{e\in E^*(\gamma)} \log \pi_{l[e]}.$$

The terms $-\log\pi_{l[e]}$ represent the energy needed to create the edges. We prefer to use the term polygonal field because the consistent fields to be considered shortly are inspired by the Arak–Surgailis polygonal Markov fields in the continuum, and more importantly, because the graph-theoretical formulation leads us to define novel simulation techniques for discrete random fields.

A careful choice of Hamiltonian in (1) leads to consistent polygonal fields. Recall that k is the number of colour labels.

Definition 4. Let $\alpha_V \in [0,1]$ and set

$$\alpha_X = 1-\alpha_V; \quad \alpha_T = \frac{1}{2}\left(1 - \frac{k-2}{k-1}\alpha_X\right); \quad \epsilon = \frac{\alpha_V}{k-1} + \frac{k-2}{k-1}\alpha_T.$$

Define

$$\begin{aligned}\Phi_D(\hat{\gamma}) \;=\; & -N_V(\gamma)\log\alpha_V - N_T(\gamma)\log((k-1)\alpha_T) \\ & -N_X(\gamma)\log((k-1)\alpha_X) + \mathrm{card}(E(\gamma))\log(k-1) \\ & -\sum_{e\in E(\gamma)}\sum_{l\in\mathcal{T},\, l\nsim e}\log(1-\epsilon\pi_l) + \sum_{n(l_1,l_2)\in\gamma}\log\left(1-\frac{\alpha_V}{k-1}\pi_{l_1}\pi_{l_2}\right).\end{aligned} \tag{3}$$

Here, N_V, N_T and N_X denote the number of V-, T- and X-vertices, $\mathrm{card}(E(\gamma))$ is the number of edges in γ, $n(l_1,l_2) \in \gamma$ ranges through the nodes of $\mathcal{T}$ that either lie on edges of γ or coincide with one of its vertices and $l \nsim e$ means that the line l intersects but is not collinear with e. We use the convention that $0\times\infty = 0$.

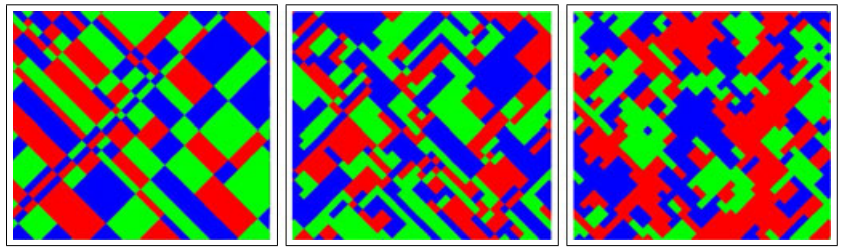

Fig. 2. Realisations of $\hat{\mathcal{A}}_{\Phi_D}$ with $\alpha_V = 0$ (left), $\alpha_V = 1/2$ (centre) and $\alpha_V = 1$ (right). In all panels, the number of colour labels is three.

A few remarks are in order. The parameter α_V controls the relative frequency of V-vertices, α_T and α_X that of vertices of degrees three and four, respectively, in a manner that will be made explicit in the dynamic representation to be derived in Section 3. These parameters are not independent and, given the number of colours k, α_T and α_X are uniquely determined by α_V. Typical realizations for $k = 3$ and α_V equal to 0, $1/2$ and 1 are shown in Figure 2. In the left-most panel, $\alpha_V = 0$ and there are no vertices having degree two; in the right-most panel, $\alpha_X = 0$ so that no vertices have degree four. The central panel displays a coloured configuration with vertices of all degrees. Visually, the three patterns are strikingly different.

Let us consider the special case $k = 2$ and $\alpha_V = 1$. First, note that the family $\hat{\Gamma}_D(\mathcal{T})$ of admissible coloured polygonal configurations does not include any member with an interior vertex of degree three. Therefore, $N_T \equiv 0$ almost surely. Moreover, as $\alpha_X = 1 - \alpha_V = 0$, the probability of any $\hat{\gamma}$ that contains X-vertices is zero. Hence, almost surely, all interior vertices have degree two and $E^*(\gamma) = E(\gamma)$. Moreover, $\log(k-1) = \log \alpha_V = 0$, $\epsilon = 1$, and (3) simplifies to

$$\Phi_D(\hat{\gamma}) = -\sum_{e \in E(\gamma)} \sum_{l \in \mathcal{T},\, l \asymp e} \log(1 - \pi_l) + \sum_{n(l_1, l_2) \in \gamma} \log\left(1 - \pi_{l_1} \pi_{l_2}\right),$$

cf. Schreiber & Van Lieshout (2010).

For the special Hamiltonian $\mathcal{H}_D = \Phi_D$ of Definition 4, the following result holds.

Theorem 1. *The polygonal field $\hat{\mathcal{A}}_{\Phi_D}$ is consistent: for bounded open convex $D' \subseteq D \subseteq \mathbb{R}^2$, the field $\hat{\mathcal{A}}_{\Phi_D} \cap D'$ coincides in distribution with $\hat{\mathcal{A}}_{\Phi_{D'}}$.*

By letting D increase to $\mathbb{R}^2$, Kolmogorov's theorem implies the existence of a whole plane extension of the process $\hat{\mathcal{A}}_\Phi$ such that the distribution of $\hat{\mathcal{A}}_{\Phi_D}$ coincides with that of $\hat{\mathcal{A}}_\Phi \cap D$ for all bounded open convex $D \subseteq \mathbb{R}^2$. The proof of Theorem 1 relies on a dynamic representation, which is the topic of the next section.

3. Dynamic representation of consistent polygonal fields

Below, we present a dynamic representation for $\hat{\mathcal{A}}_{\Phi_D}$ in analogy with the corresponding representation in Sections 4 and 5 of Arak & Surgailis (1989). The idea underlying this construction is to represent the edges of the polygonal field as the trajectory of a one-dimensional particle system evolving in time. More specifically, we interpret D as a set of time-space points $(t, y) \in D \subset \mathbb{R}^2$ and refer to t as the time coordinate, to y as the (one-dimensional) spatial coordinate of a particle. In this language, a straight line segment in D stands for a piece of the time-space trajectory of a moving particle. Compared with the bicoloured case discussed by

Schreiber & Van Lieshout (2010), note that in the current multicolour context, in general, it is not sufficient to consider colourless graphs only and assign colourings with equal probability afterwards. Moreover, the interaction structure is not restricted to a hard core condition.

For convenience, we assume that no line in $\mathcal{T}$ nor any segment of ∂D is parallel to the spatial axis. Because we might simply rotate the coordinate system otherwise, these assumptions do not lead to a loss of generality. Recall that by assumption, each line l of $\mathcal{T}$ intersects the boundary at two points. The two intersection points are ordered according to time, and the one with the smaller time coordinate is denoted $\mathrm{in}(l, D)$. Furthermore, no three lines of a regular linear tessellation intersect in a single point.

To define the dynamics, the left-most point of $\bar{D}$ is assigned a random colour chosen uniformly from the k possibilities. Let particles be born independently of other particles

- with probability $\alpha_V \pi_{l_1} \pi_{l_2}/(k-1)$ at each node $n(l_1, l_2)$, that is, the intersection of two lines l_1 and l_2 in $\mathcal{T}$, which falls in D (interior birth site);
- with probability $\pi_l/(1+\pi_l)$ at each entry point $\mathrm{in}(l, D)$ of a line $l \in \mathcal{T}$ into D (boundary birth site).

In particle system parlance, if the coordinates of the birth site are (t, y), one or more particles are born at time t at location y and start moving in $\mathbb{R}$ as follows. Each interior birth site $n(l_1, l_2)$ emits two particles moving with initial velocities such that the initial segments of their time-space trajectories lie on the lines l_1 and l_2 of the tessellation that emanate from the birth site, unless another particle (either a single one or two colliding particles) previously born hits the site, in which case the birth does not occur. Each boundary birth site $\mathrm{in}(l, D)$ emits a single particle moving with initial velocity such that the initial segment of its trajectory lies on l. Note that no precaution similar to the one for interior birth sites previously mentioned is needed because boundary birth sites cannot be hit by previously born particles. The initial time-space trajectory or trajectories of a birth event bound a new polygonal region, the colour of which is chosen uniformly from the $k-1$ colours that differ from that of the polygon just prior to the birth, or in other words, lying to the left of the birth site.

All particles evolve independently in time according to the following rules.

(**E1**) Between the critical moments listed in the succeeding text, each particle moves with constant velocity.

(**E2**) When a particle hits the boundary ∂D, it dies.

(**E3**) In case of a collision of two particles, that is, equal spatial coordinates y at some time t with $(t, y) = n(l_i, l_j) \in D$, distinguish the following cases.

(**a**) If the colours above and below (t, y) are identical, say i, with probability α_V, both particles die. With probability α_X both particles survive to create a new polygon whose colour is chosen uniformly from those not equal to i (cf. Figure 3).

(**b**) If the colours above and below (t, y) are different, say i and j, with probability α_T, each of the two particles survives whereas the other dies. With probability $(k-2)\alpha_X/(k-1) = 1 - 2\alpha_T$, both particles survive to create a new polygon whose colour is chosen uniformly from those not equal to either i or j (cf. Figure 3).

Recall that a collision prevents a birth from happening at the node.

(**E4**) Whenever a particle moving in time-space along $l_i \in \mathcal{T}$ reaches a node $n(l_i, l_j)$, it changes its velocity so that its time-space trajectory lies along l_j with probability $\alpha_V \pi_{l_j}/(k-1)$; it splits into two particles whose trajectories lie along l_i and l_j with probability $(k-2)\alpha_T \pi_{l_j}/(k-1)$ and keeps moving along l_i otherwise (with probability

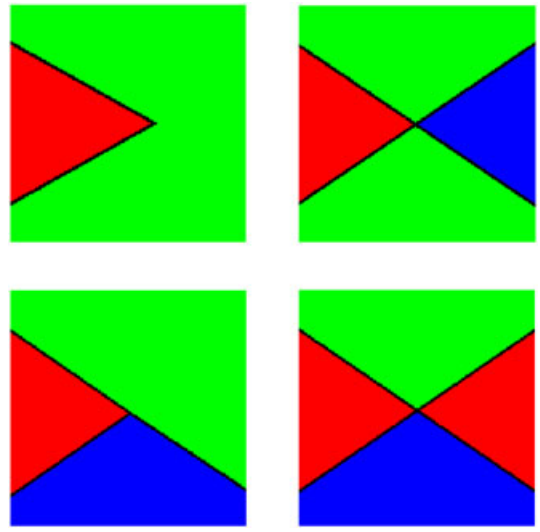

Fig. 3. Time-space trajectories of moving particles with time running from left to right. Top row (**(E3a)**): in the left-most panel, both particles die upon collision; they survive in the panel on the right, and their time-space trajectories form a new polygon coloured blue. Bottom row (**(E3b)**): in the left-most panel, one particle survives the collision; both particles survive in the panel on the right, and their time-space trajectories form a new polygon coloured red.

Fig. 4. **(E4)**: Velocity update (left), split (middle) and continuation (right) of a time-space trajectory outlined in red. Time runs from left to right.

$1-\epsilon\pi_{l_j}$). In case of a split, a new polygon is created whose colour is chosen uniformly from the $k-2$ possibilities. See Figure 4.

The dynamics described previously define a random coloured polygonal configuration $\hat{\mathcal{D}}_D$ with realizations in $\hat{\Gamma}_D(\mathcal{T})$. The key observation is that its distribution is identical to that of $\hat{\mathcal{A}}_{\Phi_D}$.

Theorem 2. *The random elements $\hat{\mathcal{A}}_{\Phi_D}$ and $\hat{\mathcal{D}}_D$ coincide in distribution.*

Proof. In order to calculate the probability that some $\hat{\gamma} \in \hat{\Gamma}_D(\mathcal{T})$ is generated by the particle dynamics **(E1)–(E4)**, observe that

- each edge $e \in E(\gamma)$ whose initial (lower time coordinate) vertex lies on ∂D yields a factor $\pi_{l[e]}/(1+\pi_{l[e]})$ (boundary birth site) times $\prod_{l\in\mathcal{T},\, l\nsim e}(1-\epsilon\pi_l)$ (no velocity/split updates along e) times $1/(k-1)$ for the colour;

- the two edges $e_1, e_2 \in E(\gamma)$ emanating from a common interior birth site $n(l_1, l_2)$ yield a factor $\alpha_V \pi_{l_1} \pi_{l_2}/(k-1)$ (the birth probability) times $\prod_{i=1}^{2} \prod_{l \in \mathcal{T},\, l \nsim e_i} (1 - \epsilon \pi_l)$ (no velocity/split updates along e_i) times $1/(k-1)$ for the colour;
- each edge $e \in E(\gamma)$ arising because of a velocity update yields a factor $\alpha_V \pi_{l[e]}/(k-1)$ (velocity update probability) times $\prod_{l \in \mathcal{T},\, l \nsim e} (1 - \epsilon \pi_l)$ (no velocity/split updates along e);
- the two edges $e_1, e_2 \in E(\gamma)$ arising from a split at node $n(l_1, l_2)$ where e_1 is a continuation and e_2 is a new direction yield a factor $(k-2)\alpha_T \pi_{l_2}/(k-1)$ (the split probability) times $\prod_{i=1}^{2} \prod_{l \in \mathcal{T},\, l \nsim e_i} (1 - \epsilon \pi_l)$ (no velocity/split updates along e_i) times $1/(k-2)$ for the colour;
- the two edges $e_1, e_2 \in E(\gamma)$ arising because of an X-collision contribute a factor $\alpha_X/(k-1)$ times $\prod_{i=1}^{2} \prod_{l \in \mathcal{T},\, l \nsim e_i} (1 - \epsilon \pi_l)$ (no velocity/split updates along e_i);
- each edge e emanating from a T-collision contributes a factor α_T times $\prod_{l \in \mathcal{T},\, l \nsim e} (1 - \epsilon \pi_l)$ (no velocity/split updates along e);
- each collision of V-type contributes a factor α_V;
- the colour choice for the left-most point of $\bar{D}$ contributes a factor $1/k$;
- the absence of birth sites in nodes $n(l_1, l_2) \in D$ that do not belong to γ yields the factor $\prod_{n(l_1,l_2) \in D \setminus \gamma} (1 - \alpha_V \pi_{l_1} \pi_{l_2}/(k-1))$;
- the absence of boundary birth sites at those entry points into D of lines of $\mathcal{T}$ which do not give rise to an edge of γ yields the factor $\prod_{l \in \mathcal{T},\, l \cap D \neq \emptyset,\, \mathrm{in}(l,D) \notin \gamma} (1 + \pi_l)^{-1}$.

Collecting all factors implies that the probability of $\hat{\gamma}$ is

$$\left(\prod_{e \in E(\gamma)} \prod_{l \in \mathcal{T},\, l \nsim e} (1 - \epsilon \pi_l) \right) \left(\prod_{n(l_1,l_2) \in D \setminus \gamma} \left(1 - \frac{\alpha_V}{k-1} \pi_{l_1} \pi_{l_2} \right) \right)$$

times

$$\left(\prod_{l \in \mathcal{T},\, l \cap D \neq \emptyset} \frac{1}{1 + \pi_l} \right) \left(\prod_{e \in E^*(\gamma)} \pi_{l[e]} \right) \left(\prod_{e \in E(\gamma)} \frac{1}{k-1} \right)$$

times

$$\frac{1}{k} \alpha_V^{N_V} \ (\alpha_T (k-1))^{N_T} \ (\alpha_X (k-1))^{N_X}, \tag{4}$$

which completes the proof. □

As an immediate consequence of the proof of Theorem 2, we obtain an explicit and simple expression for the partition function.

Corollary 1. *The partition function (2) of $\hat{\mathcal{A}}_{\Phi_D}$ is given by*

$$k \prod_{l \in \mathcal{T},\, l \cap D \neq \emptyset} (1 + \pi_l) \prod_{n(l_1,l_2) \in D} \left(1 - \frac{\alpha_V}{k-1} \pi_{l_1} \pi_{l_2} \right)^{-1}.$$

Proof. Upon dividing (4) by $\exp(-\Phi_D(\hat{\gamma}))$ with Φ_D given by (3) and the product of the activity parameters $\prod_{e \in E^*(\gamma)} \pi_{l[e]}$, which together form the numerator in (1), one is left with

$$\frac{1}{k}\prod_{n(l_1,l_2)\in D\setminus\gamma}\left(1-\frac{\alpha_V}{k-1}\pi_{l_1}\pi_{l_2}\right)\prod_{l\in\mathcal{T},\,l\cap D\neq\emptyset}\frac{1}{1+\pi_l}\prod_{n(l_1,l_2)\in\gamma}\left(1-\frac{\alpha_V}{k-1}\pi_{l_1}\pi_{l_2}\right),$$

the reciprocal of the partition function. □

Having established a proper dynamic representation, Theorem 1 follows from Theorem 2 in complete analogy with the proof of Thm. 5.1 of Arak & Surgailis (1989) as in Thm. 1 of Schreiber & Van Lieshout (2010).

Proof of Theorem 1. Choose a bounded open convex set $D \subseteq \mathbb{R}^2$ and a straight line l intersecting D, and define D' to be the set of points of D lying to the left of l (lower time coordinates). The dynamic representation implies the consistency statement for these D and D'. Noting that the dynamic representation is equally available upon rotating the time-space coordinate system, we see that the consistency holds as well upon cutting off the part of the set D lying to the left of l. This means, however, that the consistency holds upon cutting off pieces of the original set with arbitrary straight lines. A repetitive use of this procedure and a possible passage to the limit allows us to carve from D any arbitrary convex subset. □

A discrete analogue of the Poisson line transect property (Arak & Surgailis, 1989, Thm. 5.1.c) holds as well. Indeed, combining consistency with the boundary birth mechanism of the dynamic representation, we obtain the following.

Corollary 2. *Let l be a straight line that contains no nodes of $\mathcal{T}$. Then, the intersection points and intersection directions of l with the edges of the polygonal field $\hat{\mathcal{A}}_\Phi$ coincide in distribution with the intersection points and directions of l with the line field $\Lambda_\mathcal{T}$ defined to be the random subcollection of $\mathcal{T}$ where each straight line $l^* \in \mathcal{T}$ is chosen to belong to $\Lambda_\mathcal{T}$ with probability $\pi_{l^*}/(1+\pi_{l^*})$, rejected otherwise, and all these choices are made independently.*

To conclude this section, we turn to Markov properties that are direct consequences of the dynamic representation.

A spatial Markov property reminiscent of that enjoyed by the Arak–Clifford–Surgailis model in the continuum is the following. For a piece-wise smooth simple closed curve $\theta \subset \mathbb{R}^2$ containing no nodes of $\mathcal{T}$, the conditional distribution of $\hat{\mathcal{A}}_\Phi$ in the interior of θ depends on the configuration exterior to θ only through the intersections of θ with the edges of the polygonal field and through the colouring of the field along θ.

To relate our model to Gibbs fields commonly used in image analysis, assume for simplicity that $\mathcal{T}$ forms a regular lattice and D is an $m \times n$ rectangle. In this case, D is divided by $\mathcal{T}$ in square cells, known as pixels. Note that there is a one-to-one correspondence between a coloured polygonal configuration $\hat{\gamma}$ and the array of pixel colours. Indeed, the colour of a pixel is that of the face of $\hat{\gamma}$ that it falls in, and, reversely, the edges of γ are composed of the segments between pixels of different colours. In this dual framework, we obtain the following local Markov factorization.

Corollary 3. *Let D be an $m \times n$ array, and let $\mathcal{T} = \{l_1, \ldots, l_{m+n-2}\}$ be the corresponding regular linear tessellation with the indices chosen in such a way that for $i = 1, \ldots, n-1$, l_i is the horizontal line between the i-th and $(i+1)$-st row, and for $i = 1, \ldots, m-1$, l_{n+i-1} is the vertical line between the i-th and $(i+1)$-st column. Then, the random element $\hat{\mathcal{A}}_{\Phi_D}$ is the dual of a random vector $X = (X_1, \ldots, X_{mn})$ of pixel values indexed in column major order*

with a joint probability mass function $\mathbb{P}(\hat{\mathcal{A}}_{\Phi_D} = \hat{\gamma}) = \mathbb{P}(X_1 = x_1; \cdots; X_{mn} = x_{mn})$ *that factorizes as*

$$\begin{aligned}\mathbb{P}(X_1 = x_1) &\times \prod_{i=2}^{n} \mathbb{P}(X_i = x_i \mid X_{i-1} = x_{i-1}) \\ &\times \prod_{i=1}^{m-1} \mathbb{P}(X_{in+1} = x_{in+1} \mid X_{(i-1)n+1} = x_{(i-1)n+1}) \\ &\times \prod_{i=1}^{m-1} \prod_{j=2}^{n} \mathbb{P}\big(X_{in+j} = x_{in+j} \mid X_{(i-1)n+j-1} = x_{(i-1)n+j-1}; \\ &\qquad X_{(i-1)n+j} = x_{(i-1)n+j}; X_{in+j-1} = x_{in+j-1}\big)\end{aligned}$$

for $x_i \in \{1, \ldots, k\}$, $i = 1, \ldots, mn$. *Here,* $\hat{\gamma}$ *and* $(x_1, \ldots, x_{mn})$ *are dual realizations.*

Proof. Choose the time direction in the dynamic representation in such a way that the chronological order of the nodes coincides with the column major order, and recall that the conditional behaviour at a node depends only on the colours and trajectories immediately to its 'left', that is, immediately prior to it in time. For the first pixel, $\mathbb{P}(X_1 = x_1)$ is the probability that the left-most colour is x_1, which is $1/k$ as this colour is chosen uniformly from the set $\{1, \ldots, k\}$. Next, the probabilities of the pixel values in the first column are derived from the boundary birth mechanism. Thus, for $x_i, x_{i-1} \in \{1, \ldots, k\}$ and $i = 2, \ldots, n$,

$$\mathbb{P}(X_i = x_i \mid X_{i-1} = x_{i-1}) = \begin{cases} \frac{1}{k-1} \frac{\pi_{l_{i-1}}}{1+\pi_{l_{i-1}}} & \text{if } x_i \neq x_{i-1}; \\ \frac{1}{1+\pi_{l_{i-1}}} & \text{if } x_i = x_{i-1}. \end{cases}$$

Similarly, for $x_{in+1}, x_{(i-1)n+1} \in \{1, \ldots, k\}$ and $i = 1, \ldots, m-1$,

$$\mathbb{P}(X_{in+1} = x_{in+1} \mid X_{(i-1)n+1} = x_{(i-1)n+1}) = \begin{cases} \frac{1}{k-1} \frac{\pi_{l_{i+n-1}}}{1+\pi_{l_{n+i-1}}} & \text{if } x_{in+1} \neq x_{(i-1)n+1}; \\ \frac{1}{1+\pi_{l_{n+i-1}}} & \text{if } x_{in+1} = x_{(i-1)n+1}. \end{cases}$$

Use the shorthand notation $\mathbb{P}_{ij}(x \mid u, v, w)$ for

$$\mathbb{P}(X_{in+j} = x_{in+j} \mid X_{(i-1)n+j-1} = u; X_{(i-1)n+j} = v; X_{in+j-1} = w).$$

Then, for $u \neq v \neq w \neq u$,

$$\mathbb{P}_{ij}(x \mid u, v, v) = \begin{cases} \alpha_V & \text{if } x = v \\ \alpha_X/(k-1) & \text{if } x \neq v \end{cases}$$

by **(E3a)**, and

$$\mathbb{P}_{ij}(x \mid u, v, w) = \begin{cases} \alpha_T & \text{if } x \in \{v, w\} \\ \alpha_X/(k-1) & \text{if } x \notin \{v, w\} \end{cases}$$

by **(E3b)** regardless of i, j. Furthermore, the interior birth mechanism implies that

$$\mathbb{P}_{ij}(x \mid u,u,u) = \begin{cases} \alpha_V \pi_{l_{j-1}} \pi_{l_{n+i-1}}/(k-1)^2 & \text{if } x \neq u \\ 1 - \alpha_V \pi_{l_{j-1}} \pi_{l_{n+i-1}}/(k-1) & \text{if } x = u \end{cases}$$

and finally, **(E4)** determines the probabilities

$$\mathbb{P}_{ij}(x \mid u,u,v) = \begin{cases} 1 - \epsilon \pi_{l_{j-1}} & \text{if } x = v \\ \alpha_V \pi_{l_{j-1}}/(k-1) & \text{if } x = u \\ \alpha_T \pi_{l_{j-1}}/(k-1) & \text{if } x \notin \{u,v\} \end{cases}$$

and

$$\mathbb{P}_{ij}(x \mid u,v,u) = \begin{cases} 1 - \epsilon \pi_{l_{n+i-1}} & \text{if } x = v; \\ \alpha_V \pi_{l_{n+i-1}}/(k-1) & \text{if } x = u; \\ \alpha_T \pi_{l_{n+i-1}}/(k-1) & \text{if } x \notin \{u,v\}. \end{cases}$$

Collecting all terms completes the proof. □

Models for which the previous factorization holds were dubbed 'mutually compatible Gibbs random fields' by Goutsias (1989). In particular, the interior birth mechanism, as well as the collisions and path propagation described in the dynamic representation's **(E3)–(E4)** correspond to the local transfer function of Goutsias (1989), see also Champagnat *et al.* (1998).

Note that we have chosen the time direction so as to conform to column major order. A fortiori, such models are Markov random fields with the second order neighbourhood structure in which horizontally, vertically and diagonally adjacent pixels are neighbours.

A factorization similar to that in Corollary 3 holds for any regular linear tessellation $\mathcal{T}$, any choice of time axis and any bounded open convex set D. Indeed, because of the assumptions on $\mathcal{T}$, every interior node is hit by exactly two segments that are adjacent to three cells (pixels) in $\mathcal{D}_{\mathcal{T}}$. These pixels are not necessarily rectangular. See Figure 6 for an example. The notation, however, tends to become cumbersome. For this reason, we prefer to use the graph-theoretical formulation with its neater formulae.

4. Birth and death dynamics

In this section, we use the dynamic representation of Section 3 to propose dynamics that are reversible and leave the law of $\hat{\mathcal{A}}_{\Phi_D}$ invariant. These dynamics will serve as stepping stone for building Metropolis–Hastings dynamics for the general polygonal field models (1). For the two-colour case, algorithms inspired by dynamic representations can be found in Kluszczyński *et al.* (2005), Matuszak & Schreiber (2012), Schreiber (2005) and Schreiber & Van Lieshout (2010). In that case, however, it is sufficient to focus on colour-blind polygonal configurations as the colouring is completely determined by the colour at a single point. For $k > 2$, this is no longer the case and we have to explicitly incorporate colours in our dynamics. Moreover, particles do not necessarily die upon collision, and the disagreement loop principle of Schreiber (2005) no longer applies.

The basic continuous time dynamics we propose consist of adding and deleting particle birth sites, either at internal nodes $n(l_1, l_2)$ or at entry points $\mathrm{in}(l, D)$ on ∂D. Nodes that are not a birth site will be called vacant. In order to fully explore the state space, recolouring will also be necessary, at some fixed rate $\tau > 0$. We work with a constant death rate 1. Thus, our dynamics allow for both local (recolouring) updates and global changes (the addition or deletion of a birth site).

The birth rate at a boundary entry point in(l, D) and a vacant internal node $n(l_1, l_2)$ are set to π_l and $\alpha_V \pi_{l_1} \pi_{l_2}/(k - 1 - \alpha_V \pi_{l_1} \pi_{l_2})$ to satisfy the detailed balance equations

$$\frac{\pi_l}{1 + \pi_l} \times 1 = \left(1 - \frac{\pi_l}{1 + \pi_l}\right) \times \text{birth rate}(\text{in}(l, D))$$

respectively

$$\frac{\alpha_V}{k - 1} \pi_{l_1} \pi_{l_2} \times 1 = \left(1 - \frac{\alpha_V}{k - 1} \pi_{l_1} \pi_{l_2}\right) \times \text{birth rate}(n(l_1, l_2)).$$

Recall that if $n(l_1, l_2)$ is hit by some previously born particle, the birth is discarded. For computational convenience, we shall keep track of the discarded births during the dynamics.

In case of a birth update, the particle(s) emitted at the birth site are given time-space trajectories in accordance with **(E4)**. Upon collisions, **(E3)** is invoked. Whenever possible, existing trajectories are re-used. A dual reasoning is applied to deaths.

To make the previous ideas precise, suppose that the current state is $\hat{\gamma}$, understood here to *include* the knowledge of all discarded birth sites, which we modify by adding or deleting a (discarded) birth site to obtain $\hat{\gamma}'$. We shall use the following segment classification.

plus the segment does not lie on any edge of γ, but it does lie on some edge of γ';
minus the segment lies on some edge of γ, but it does not lie on any edge of γ';
changed the segment lies on some common edge of γ and γ', but the colour of at least one of its adjacent polygonal faces has changed, or the segment lies in the interior of faces of $\hat{\gamma}$ and $\hat{\gamma}'$ having different colours.

The dynamics are now as follows. In case of a birth at node $n(l_1, l_2)$ with coordinates (t, y), two plus segments arise along l_1 and l_2 forward in time. In case of a boundary birth, a single plus segment is generated. Similarly, in case of a death, one or two minus segments arise. We order the nodes with first coordinate larger than t in chronological order and update them one at a time until some further time $t' > t$ for which the intersections of $\hat{\gamma}$ and $\hat{\gamma}'$ with the vertical line specified by first coordinate t' are identical.

At each node, we first check whether the node is hit either by some segment marked 'plus' or 'minus' or by some 'changed' segment of γ. How to update $\hat{\gamma}$ to obtain $\hat{\gamma}'$ is summarized in Tables 1–2 and described in the succeeding text .

If no such segment exists, we need to check whether the node is a non-discarded birth site. If it is, due to, for example, nesting, the colour just prior to the birth site may be different in $\hat{\gamma}$ and $\hat{\gamma}'$. In this case, a new colour is chosen in $\hat{\gamma}'$ for the region to the right of the node from those not equal to the colour just prior to the node (in $\hat{\gamma}'$). In all other cases, the status quo is propagated.

If the node is hit by two marked segments ('plus', 'minus' or 'changed' and belonging to γ), or by one such segment and one that is an unchanged common edge of γ and γ', which we label 'old', a collision update is made as outlined in Table 1.

In the remaining case that the node is hit by a single segment marked either 'plus' or 'minus' or by a segment of γ labelled 'changed', the path is updated as outlined in Table 2.

An illustration is given in Figure 5. The current node n to be updated is in the middle of the panels. In $\hat{\gamma}$, the node is a birth site; no segments hit n, and there are two emanating segments. In the new polygonal configuration $\hat{\gamma}'$, the node is hit by a segment separating the green from the blue face which is therefore labelled 'plus'. According to Table 2, in $\hat{\gamma}'$, the birth gets discarded and we invoke **(E4)**, say resulting in the decision to split. Hence, we must also choose a colour other than green or blue for the region to the right, that is, forwards in time, for example red.

Table 1. *Collision updates*

minus/minus at vacant node	label emanating segments;
minus/minus at discarded birth site	implement birth by choosing new colour from those not equal to that prior to the discarded birth site; label emanating segments;
minus/old minus/plus minus/changed	invoke **(E4)**; label emanating segments;
plus/old plus/changed old/changed plus/plus at vacant node	invoke **(E3)**; label emanating segments;
plus/plus at birth site	discard the birth; invoke **(E3)** and label emanating segments;
changed/changed	check whether the colours above and below the face bounded by the two hitting segments agree in $\hat{\gamma}$ and $\hat{\gamma}'$; if so, do nothing; otherwise invoke **(E3)** and label emanating segments.

Table 2. *Path updates*

plus path at birth site	discard the birth; invoke **(E4)**; label emanating segments;
plus path at vacant site	invoke **(E4)**; label emanating segments;
minus path at discarded birth site	implement birth by choosing new colour from those not equal to that prior to the discarded birth site; label emanating segments;
minus path at vacant site	label emanating segments;
changed path	in case the path splits, choose a new colour from those not equal to the colours above and below the path; label emanating segments.

The labels of the two emanating segments are 'changed' for the one separating the blue and red faces, and 'old' for the one forming the boundary between the red and green faces.

For recolouring, classic local colour switches are used, as detailed in for example Winkler (2003). As for the two-colour case in Schreiber & Van Lieshout (2010), we obtain the following result.

Theorem 3. *The distribution of the consistent polygonal field* $\hat{\mathcal{A}}_{\Phi_D}$ *is the unique invariant probability distribution of the birth-death-recolour dynamics described previously upon ignoring discarded birth attempts, to which they converge in total variation from any initial state* $\hat{\gamma} \in \hat{\Gamma}_D(\mathcal{T})$ *for which* $\mathbb{P}(\hat{\mathcal{A}}_{\Phi_D} = \hat{\gamma}) > 0$.

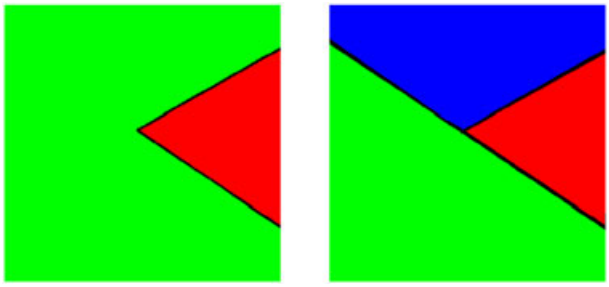

Fig. 5. Left: $\hat{\gamma}$. Right: $\hat{\gamma}'$.

Proof. The case $k = 2$ was considered in Schreiber & Van Lieshout (2010). Hence, assume that $k > 2$. The total transition rate of the birth-death-recolour dynamics is bounded from above by a positive constant. Indeed, for each internal birth site $n(l_1, l_2)$, the rate

$$\frac{\alpha_V \pi_{l_1} \pi_{l_2}/(k-1)}{1-\alpha_V \pi_{l_1} \pi_{l_2}/(k-1)} \leq \frac{1/(k-1)}{1-1/(k-1)} = \frac{1}{k-2} \leq 1.$$

The death rate for a (discarded) birth at $n(l_1, l_2)$ is equal to 1. Similarly, the birth rate π_l at entry points $\mathrm{in}(l, D)$ is bounded from above by 1, and the death rate is equal to 1. Therefore, an upper bound to the total transition rate is the sum of the recolouring rate τ, the number of nodes and the number of lines hitting D. Thus, our dynamics can be algorithmically generated by a Poisson clock of constant rate, and an embedded Markov transition matrix that governs the transitions. This transition matrix restricted to admissible coloured polygonal configurations which, upon including discarded birth attempts, have positive probability under its putative limit distribution is irreducible, because any state can be reached from any other state by successively removing all (discarded) birth attempts, choosing an appropriate colour for the left-most point of D and then building the target state by successively adding particles. Hence, the dynamics constitute a finite state space irreducible Markov process, and there exists a unique invariant probability distribution. See for example Theorem 20.1 in Levin *et al.* (2008). The same theorem also yields the convergence in total variation. The invariance of the distribution of $\hat{\mathcal{A}}_{\Phi_D}$ augmented with the knowledge of discarded birth attempts follows from the invariance of the Bernoulli birth site probabilities under the dynamics, the fact that the trajectories preserve **(E1)–(E4)** by design, and the well-known invariance of the local colour switches (Winkler, 2003, Section 10.2). Taking the marginal distribution of $\hat{\mathcal{A}}_{\Phi_D}$ by integrating out the probabilities of nodes being traced by previously born particles being birth sites or not (which sum to one) completes the proof. □

In fact, the dynamics are reversible. Consider for example the collision of a positive path with a birth site as in Figure 5. In this example, the transition rate is multiplied by $(k-2)\alpha_T \pi_{l_j}/(k-1)$ for the split and $1/(k-2)$ for the colour, amounting to $\alpha_T \pi_{l_j}/(k-1)$, whereas the probability of $\hat{\gamma}$ *including the knowledge of discarded births* gains a factor $(k-1)\alpha_T \pi_{l_j}/(k-1) = \alpha_T \pi_{l_j}$ (the first term $k-1$ to compensate for the choice of colour in $\hat{\gamma}$, the second for the split and colour in $\hat{\gamma}'$). The reverse collision of a minus path with a discarded birth site yields a factor $1/(k-1)$ for the rate. Thus, this type of collision is reversible. Similar calculations can be made for the other types of collision and are left to the reader.

For general polygonal field models (1) with a Hamiltonian $\mathcal{H}_D$ that is the sum of (3) and some other term Ψ_D, we propose a Metropolis–Hastings algorithm. The algorithm has the same birth, death and recolour rates as the dynamics presented in Section 4. The difference is that a new state $\hat{\gamma}'$ is accepted with probability

$$\min\left(1, \exp\left[\Psi_D(\hat{\gamma}) - \Psi_D(\hat{\gamma}')\right]\right), \tag{5}$$

whereas the old state is kept with the complementary probability. An example of Ψ_D will be presented in Section 5.

Theorem 4. *Let $\Psi_D : \hat{\Gamma}_D(\mathcal{T}) \mapsto \mathbb{R}$ be finite. Then, the distribution of the polygonal field $\hat{\mathcal{A}}_{\Phi_D+\Psi_D}$ is the unique invariant probability distribution of the Metropolis–Hastings dynamics (5) upon ignoring discarded birth attempts, to which they converge in total variation from any initial state $\hat{\gamma} \in \hat{\Gamma}_D(\mathcal{T})$ for which $\mathbb{P}(\hat{\mathcal{A}}_{\Phi_D+\Psi_D} = \hat{\gamma}) > 0$.*

Proof. By the assumption on the Hamiltonian and arguments analogous to those in the proof of Theorem 3, the embedded Markov transition matrix that governs the transitions is irreducible. Hence, the dynamics constitute a finite state space irreducible Markov process, and there exists a unique invariant probability distribution, cf. Theorem 20.1 in Levin *et al.* (2008), to which they converge in total variation. By the proof of Theorem 3, the birth-death-recolour dynamics leave the distribution of $\hat{\mathcal{A}}_{\Phi_D}$ augmented with the knowledge of discarded birth attempts invariant. The modification by the acceptance probabilities (5) yields that the distribution of $\hat{\mathcal{A}}_{\Phi_D+\Psi_D}$ augmented with the knowledge of discarded birth attempts is left invariant by the Metropolis–Hastings dynamics. Summing over discarded birth attempts completes the proof. □

5. Application to linear network extraction

The goal of this section is to apply the model presented in Section 2 to the extraction of a network of tracks in between crop fields from image data. The left-most panel in Figure 6, obtained from the collection of publicly released Synthetic Aperture Radar images at the NASA/JPL web site http://southport.jpl.nasa.gov shows an agricultural region in Ukraine. A pattern of fields separated by tracks is visible, broken by some hamlets. The image was previously analyzed by Stoica *et al.* (2002) by means of a Markov line segment process.

Note that the tracks that run between adjacent fields show up in the image as whitish lines against the darker fields. Thus, a track is associated with a large value of the image gradient. To find a suitable family $\mathcal{T}$ of straight lines, we therefore begin by computing the gradient of the data image after convolution with a radially symmetric Gaussian kernel with standard deviation $\sigma = 3$ to suppress noise. The right-most panel in Figure 6 shows the gradient length thus obtained. We then compute the Hough transform (Duda & Hart 1972; Hough 1962) in an 80×80 accumulation array and select the eight lines corresponding to the bins with the largest number of accumulated votes. This collection is augmented by lines parametrized by the largest local extrema in the accumulation array to yield the 42 lines shown in the bottom panel of Figure 6. The resulting set is finite and contains no three lines that intersect in a common point, in other words, it is a regular linear tessellation. Regarding the choice of α_V, a comparison of the data with the simulations shown in Figure 2 suggests $\alpha_V = 1/2$. Because the lines are selected on the basis of a large-gradient value, there seems to be no particular reason to favour one line over another, so we may set the line activity parameters to a constant value.

To quantify how well a polygonal configuration fits the data, recall that an edge should be present when there is a large gradient, and absent when the gradient is small. This desirable property is captured by the Hamiltonian

$$\Psi_D(\hat{\gamma}) = -\beta \sum_{e \in E(\gamma)} [f(e) - c(e)], \tag{6}$$

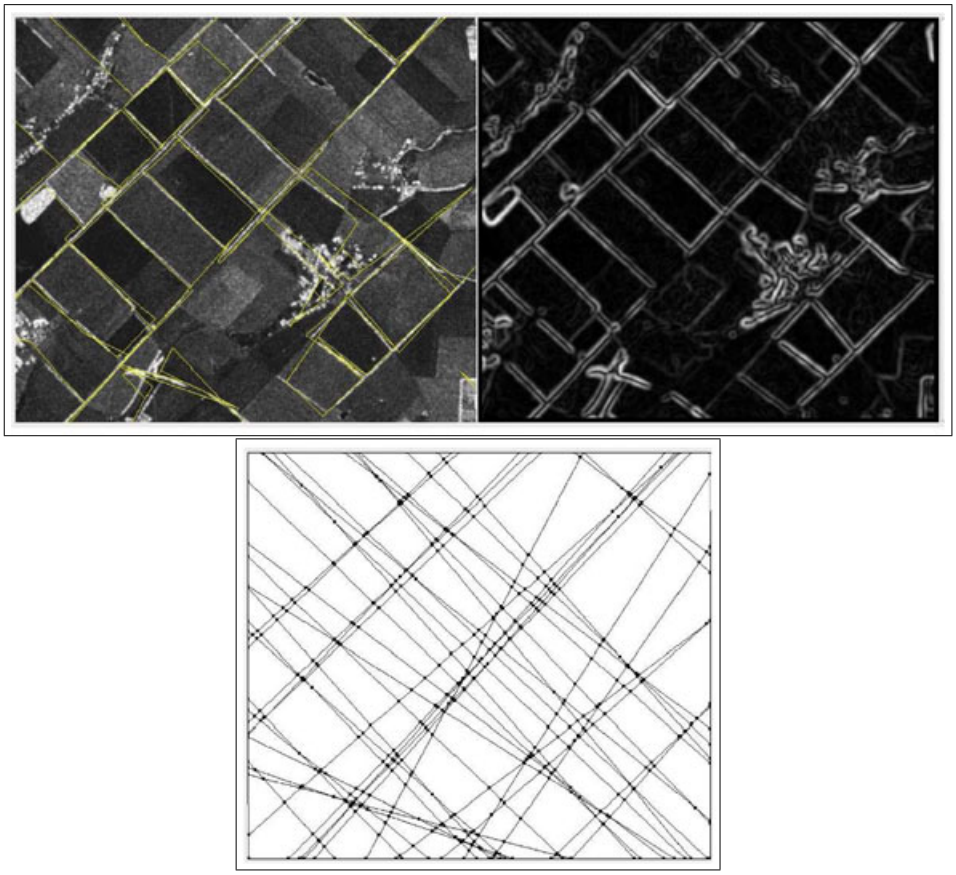

Fig. 6. Polygonal configuration (in yellow) overlaid on a Synthetic Aperture Radar image of fields in rural Ukraine (top left panel), the corresponding edge map (top right panel) and a regular linear tessellation extracted from the Hough accumulation array (bottom row).

where $f(e)$ is the integrated absolute gradient flux along edge e, $c(e)$ a threshold to discourage spurious edges and $\beta > 0$ a tuning parameter. We take $c(e)$ proportional to the number of segments along the edge with proportionality constant $c > 0$. For this choice, (6), being a sum of segment contributions, is local in nature, which is convenient from a computational perspective.

To find an optimal polygonal configuration, we use simulated annealing applied to the Metropolis–Hastings algorithm of Section 3 for $\hat{\mathcal{A}}_{\Phi_D+\Psi_D}$ with Φ_D given by (3), Ψ_D defined by (6) and recolour rate 100. Time runs from left to right after a slight rotation of the image to satisfy the condition in Section 3 that no segment of ∂D should be parallel to the spatial axis. Starting at temperature $1/\beta = 10$, the inverse temperature parameter β is slowly increased to 100 according to a geometric cooling schedule. The result for $c = 2$, line activity $1/2$ and $k = 4$ is shown in Figure 6. Note that all fields bordered by tracks are detected. A few false positives occur near the hamlets and are connected to the track network. The precision of the line placement is clearly linked to the precision of the underlying regular linear tessellation. An example of this is the border of a field near the middle of the top of the image, which is misplaced because of the fact that $\mathcal{T}$ contains no more suitable line in terms of integrated absolute gradient

flux. Naturally, one could expand the collection $\mathcal{T}$, for example, by increasing the size of the accumulation array of the Hough transform but at the expense of a higher computational cost.

6. Summary and discussion

In this paper, a new class of consistent random fields was introduced whose realizations are coloured mosaics with not necessarily convex polygonal tiles. The vertices of the polygonal tiles may have degrees two, three or four. The construction, inspired by the Arak–Clifford–Surgailis polygonal Markov fields in the continuum (Arak, 1982; Arak & Surgailis, 1989, 1991; Arak *et al.*, 1993), extends our previous construction (Schreiber & Van Lieshout 2010) of consistent polygonal random fields with tile vertices of degree two only. The latter case is substantially simpler because of the fact that interactions are restricted to a hard core constraint only, and, moreover, for a given realization, there are only two equally likely admissible colourings. We developed a dynamic representation for a class of consistent multicolour polygonal fields, which was used to prove the basic properties of the model including an explicit expression for the partition function. Local and spatial Markov properties were also considered. The dynamic representation provided the foundation on which to build Metropolis–Hastings style samplers for Gibbsian modifications of these fields. Finally, we applied the model to the detection of linear networks in rural scenes. A modification of our models would consist in ascribing activity parameters to segments rather than lines, cf. Matuszak & Schreiber (2012). A disadvantage seems to be that the dynamic representation would depend on the direction of time, in other words, the model would be anisotropic.

To conclude, we should stress that, although the model was inspired by those of Arak and co-authors, there are striking differences inherent to the discrete set-up. Notably, in the continuum, collinear edges are not allowed, in the discrete set-up, they are. Indeed, if one were to forbid collinear edges, this would lead to a forbidden line whose influence would be felt at arbitrarily large distance from its single edge, hence ruling out any meaningful Markovianity. This is not true in the continuum as the dynamic representation there ensures that collinear edges occur with probability zero. As a consequence, our consistent random fields are not Arak–Surgailis fields conditional on having their edges along the lines of $\mathcal{T}$. More fruitfully, our models provide a graph-theoretical interpretation of mutually compatible Gibbs random fields that inspires novel simulation algorithms as an alternative to the usual local tile updating schemes (Winkler 2003).

Acknowledgements

This research was supported by The Netherlands Organisation for Scientific Research NWO (613.000.809). The author is grateful to T. Schreiber for a pleasant and interesting collaboration on polygonal Markov fields and their applications that was cut short by his untimely death, to H. Noot for programming assistance, to K. Kayabol for reading a preliminary draft and to anonymous referees for their careful reading and helpful suggestions.

References

Arak, T. (1982). On Markovian random fields with finite number of values. In *4th USSR-Japan Symposium on Probability Theory and Mathematical Statistics, Abstracts of Communications*, vol. 1, 110–111, Tbilisi.

Arak, T. & Surgailis, D. (1989). Markov fields with polygonal realisations. *Probab. Theory Rel.* **80**, 543–579.

Arak, T. & Surgailis, D. (1991). Consistent Polygonal Fields. *Probab. Theory Rel.* **89**, 319–346.

Arak, T., Clifford, P. & Surgailis, D. (1993). Point-based Polygonal Models for Random Graphs. *Adv. in Appl. Probab.* **25**, 348–372.

Calka, P. (2010). Tessellations. In *New Perspectives in Stochastic Geometry* (eds W. S. Kendall & I. Molchanov), Oxford University Press, Oxford; 145–169.

Champagnat, F., Idier, J. & Goussard, Y. (1998). Stationary Markov random fields on a finite rectangular lattice. *IEEE Trans. Inform. Theory* **44**, 2901–2916.

Clifford, P. & Middleton, R. D. (1989). Reconstruction of polygonal images. *J. Appl. Stat.* **16**, 409–422.

Clifford, P. & Nicholls, G. (1994). *A Metropolis sampler for polygonal image reconstruction*. Available at: http://www.stats.ox.ac.uk/~clifford/papers/met_poly.html.

Duda, R. O. & Hart, P. E. (1972). Use of the Hough transformation to detect lines and curves in pictures. *Commun. ACM* **15**, 11–15.

Goutsias, J. K. (1989). Mutually compatible Gibbs random fields. *IEEE Trans. Inform. Theory* **35**, 1233–1249.

Hough, P. V. C. (1962). *Method and means for recognizing complex patterns*. US Patent 3069654.

Kluszczyński, R., Van Lieshout, M. N. M. & Schreiber, T. (2005). An algorithm for binary image segmentation using polygonal Markov fields. In *Image Analysis and Processing, Proceedings of the 13th International Conference on Image Analysis and Processing*, vol. 3615 (eds F. Roli & S. Vitulano), Lecture Notes in Comput. Sci. Springer, Berlin; 383–390.

Kluszczyński, R., Van Lieshout, M. N. M. & Schreiber, T. (2007). Image segmentation by polygonal Markov fields. *Ann. Inst. Statist. Math.* **59**, 465–486.

Levin, D. A., Peres, Y. & Wilmer, E. L. (2008). *Markov chains and mixing times*, American Mathematical Society, Providence.

Lieshout, M. N. M. van & Schreiber, T. (2007). Perfect simulation for length-interacting polygonal Markov fields in the plane. *Scand. J. Statist.* **34**, 615–625.

Lieshout, M. N. M. van. (2012). An introduction to planar random tessellation models. *Spatial Statistics* **1**, 40–49.

Mackisack, M. S. & Miles, R. E. (2002). A large class of random tessellations with classical Poisson polygon distributions. *Forma* **17**, 1–17.

Matuszak, M. & Schreiber, T. (2012). Locally specified polygonal Markov fields for image segmentation. In *Mathematical Methods for Signal and Image Analysis and Representation*, vol. 41 (eds L. Florack, R. Duits, G. Jongbloed, M.-C. Van Lieshout & L. Davies), Computational imaging and vision; 261–274.

Nicholls, G. K. (2001). Spontaneous magnetization in the plane. *J. Stat. Phys.* **102**, 1229–1251.

Paskin, M. A. & Thrun, S. (2005). Robotic mapping with polygonal random fields. In *Proceedings in Artificial Intelligence UAI-05*, 450–458, AUAI Press Edinburgh.

Schreiber, T. (2005). Random dynamics and thermodynamic limits for polygonal Markov fields in the plane. *Adv. in Appl. Probab.* **37**, 884–907.

Schreiber, T. (2006). Dobrushin–Kotecký–Shlosman theorem for polygonal Markov fields in the plane. *J. Stat. Phys.* **123**, 631–684.

Schreiber, T. (2008). Non-homogeneous polygonal Markov fields in the plane: graphical representations and geometry of higher order correlations. *J. Stat. Phys.* **132**, 669–705.

Schreiber, T. (2010). Polygonal web representation for higher order correlation functions of consistent polygonal Markov fields in the plane. *J. Stat. Phys.* **140**, 752–783.

Schreiber, T. & Van Lieshout, M. N. M. (2010). Disagreement loop and path creation/annihilation algorithms for binary planar Markov fields with applications to image segmentation. *Scand. J. Statist.* **37**, 264–285.

Stoica, R.S., Descombes, X., Van Lieshout, M. N. M. & Zerubia, J. (2002). An application of marked point processes to the extraction of linear networks from images. In *Spatial Statistics: Case Studies* (eds J. Mateu & F. Montes), WIT Press, Southampton; 287–312.

Thåle, C. (2011). Arak–Clifford–Surgailis tessellations. Basic properties and variance of the total edge length. *J. Stat. Phys* **144**, 1329–1339.

Weiß, V. & Cowan, R. (2011). Topological Relationships in Spatial tessellations. *Adv. in Appl. Probab.* **43**, 963–984.

Winkler, G. (2003). *Image analysis, random fields and Markov chain Monte Carlo methods: A mathematical introduction*, (2nd edn)., Applications of Mathematics, Stochastic Modelling and Applied Probability, vol. 27, Springer-Verlag, Berlin.

Received November 2012, in final form June 2013

M.N.M. van Lieshout, Centrum Wiskunde & Informatica, P.O. Box 94079, NL-1090 GB Amsterdam, the Netherlands.
E-mail: M.N.M.van.Lieshout@cwi.nl